Modeling Network for Argon Glow Discharges: The Output Cannot Be Better Than The Input

Annemie Bogaerts and Renaat Gijbels

Department of Chemistry, University of Antwerp, Universiteitsplein 1, B-2610 Wilrijk-Antwerp, Belgium

Abstract. A modeling network has been developed for Ar glow discharges with Cu cathode, consisting of several submodels, i.e., Monte Carlo simulations, fluid approaches and collisional-radiative models. The plasma species described in the models, include the electrons, Ar atoms, Ar ions, fast Ar atoms, Ar atoms in various excited levels, sputtered Cu atoms and Cu ions, both in the ground state and in various excited levels. In this paper, the models are described, and the various input data needed for the calculations are discussed. Typical results of the models include the electrical characteristics, the potential and electric field distribution, the densities, fluxes and energies of the various plasma species, information about collision processes in the plasma and about sputtering at the cathode, optical emission intensities, etc. Some of these results will be presented here, to illustrate the possibilities of the model.

INTRODUCTION

Glow discharge plasmas are used in a large number of application fields, such as in the semiconductor industry (for the deposition of thin layers and the etching of surfaces), in materials technology (for the deposition of hard coatings), in the laser and light industry, in flat plasma display panels, and also for the spectrochemical analysis of (mainly) solid materials [1]. In the latter application, the material to be analyzed is used as the cathode of the glow discharge, which is sputter-bombarded by plasma species. The sputtered cathode atoms arrive in the plasma, where their concentration can be measured with atomic absorption or fluorescence spectrometry (glow discharge atomic absorption spectrometry or fluorescence spectrometry; GD-AAS or GD-AFS). Moreover, the atoms can become ionized or excited in the plasma. The corresponding ions can be detected in a mass spectrometer (glow discharge mass spectrometry; GDMS), whereas the excited atoms and ions emit characteristic photons which can be detected with optical emission spectrometry (GD-OES).

In order to improve the results of glow discharge analytical spectrometries, we have developed a number of models to describe the behavior of various plasma species. The models can, however, also be useful for other application fields.

Different kinds of models have been used in the literature to describe glow discharge plasmas, i.e., analytical approaches, fluid models, Boltzmann equations, Monte Carlo methods and particle-in-cell simulations. All these models have their specific advantages and disadvantages. Therefore, we use a hybrid model, which is a combination of (some of) the above models for the various plasma species, in order to

CP543, *Atomic and Molecular Data and Their Applications*, edited by K. A. Berrington and K. L. Bell

combine the advantages and avoid the disadvantages of the individual models. In the following, we will give a brief description of the models and show some typical results.

DESCRIPTION OF THE MODELS

The hybrid model network is developed for an Ar plasma with a Cu cathode. The species assumed to be present in the plasma are electrons, Ar gas atoms, Ar ions, fast Ar atoms, Ar atoms in various excited levels, sputtered Cu atoms and Cu ions, in the ground state and in excited levels. These species are described with a combination of Monte Carlo simulations, fluid approaches and collisional-radiative models. Briefly, the Monte Carlo simulations are used for the "fast" plasma species, which are not in equilibrium with the electric field (such as fast electrons); the fluid approach is applied for the "slow" plasma species, which can be considered in equilibrium with the electric field (like slow electrons or Ar ions); and the collisional-radiative models describe the behavior of the atoms and ions in excited levels. An overview of the various plasma species and the models used to describe them is given in Table 1.

The Monte Carlo models are all developed in three dimensions, whereas the fluid and collisional-radiative models are two-dimensional. Indeed, the model network is generally applied to cylindrically symmetrical glow discharge cells, so that the three dimensions can be reduced to two dimensions. The model network has mainly been applied to direct current (dc) glow discharges (see e.g., [2] and references therein), but capacitively coupled radio-frequency (rf) discharges have been investigated as well ([3] and references therein), and the modeling of microsecond pulsed discharges is in progress [4]. Below, each of the models will be described in some more detail.

TABLE 1. Overview of the Different Plasma Species and the Models Used to Describe Them.

Plasma Species	Model
Ar gas atoms	no model (uniformly distributed + at rest) or: gas heating model (dc case)
fast electrons	Monte Carlo model
slow electrons	fluid model
Ar^+, Ar^{2+}, Ar_2^+ ions	fluid model
Ar^+ ions in CDS	Monte Carlo model
fast Ar atoms in CDS	Monte Carlo model
Ar atoms in various excited levels	collisional-radiative model
sputtered Cu atoms: thermalization	Monte Carlo model
Cu atoms and ions in ground state + excited levels	collisional-radiative model
Cu^+ ions in CDS	Monte Carlo model

Monte Carlo Model for the Fast Electrons

It should be mentioned that the electrons are split up in two groups, i.e., the fast and slow electrons, depending on their energy. Indeed, the electrons are called "fast" when they have enough energy to produce inelastic collisions. Since excitation and ionization of Ar ground state levels are the most frequent collision types, the threshold is in practice mostly defined at 11.55 eV (which is the lowest excited Ar level).

The fast electrons are simulated with a Monte Carlo model. A large number of electrons are followed, one after the other, during successive time-steps. Their trajectory during one time-step (Δt) is calculated with Newton's laws:

$$
\begin{aligned}
z &= z_0 + v_{z_0}\Delta t + \frac{qE_{ax}(z,r,t)}{2m}(\Delta t)^2 \\
x &= x_0 + v_{x_0}\Delta t + \frac{qE_{rad}(z,r,t)\cos(\alpha)}{2m}(\Delta t)^2 \\
y &= y_0 + v_{y_0}\Delta t + \frac{qE_{rad}(z,r,t)\sin(\alpha)}{2m}(\Delta t)^2 \\
v_z &= v_{z_0} + \frac{qE_{ax}(z,r,t)}{m}\Delta t \\
v_x &= v_{x_0} + \frac{qE_{rad}(z,r,t)\cos(\alpha)}{m}\Delta t \\
v_y &= v_{y_0} + \frac{qE_{rad}(z,r,t)\sin(\alpha)}{m}\Delta t
\end{aligned}
\qquad (1)
$$

where z_0, x_0, y_0 and z, x, y are the position coordinates before and after Δt, $v_{z_0}, v_{x_0}, v_{y_0}$ and v_z, v_x, v_y are the velocities before and after Δt, E_{ax} and E_{rad} are the axial and radial electric field, as a function of axial and radial position and time (obtained from the Ar ion - slow electron fluid model, see below), α is the azimuthal angle of the radial position (i.e. the angle of the radial position coordinates with respect to the x-axis), and q and m are the electron charge and mass, respectively.

The probability of a collision during that time-step, $Prob_{coll}$, is calculated and compared with a random number between 0 and 1:

$$Prob_{coll} = 1 - exp\left(-\Delta s \Sigma(n\sigma_{coll}(E))\right) \qquad (2)$$

where Δs is the distance traveled during Δt; n and $\sigma_{coll}(E)$ are the densities of the target particles and the cross sections of the different collision types of the electron with energy E. If the probability is lower than the random number, no collision occurs, and the Monte Carlo solver continues with the next electron during that time-step. If the probability is higher, a collision takes place. The collisions taken into account in the model, are elastic collisions with Ar ground state atoms, electron impact ionization, excitation and de-excitation for all Ar atom levels, Cu atom and Cu ion levels, and also electron-electron Coulomb scattering. Elastic collisions and electron impact excitation and ionization from the Ar ground state are the most frequent processes. Their cross sections are adopted from ref. [5]. The cross sections used for detailed electron impact ionization, excitation and de-excitation between various excited Ar atom and Cu atom and ion levels are explained in detail in refs. [6,7]. Some of these cross sections are based on experimental data, others on quantum-mechanical calculations, but most of them are obtained from empirical formulas (e.g., depending

on the energy difference between the levels), and are subject to considerable uncertainties. Nevertheless, it appeared that they have only minor effect on the final calculation results, because they determine only the level populations of the excited levels (see below) and not the overall electron behavior. Finally, the cross section for electron-electron Coulomb scattering is taken from ref. [8]. The accuracy of this cross section is again not so important for the general electron behavior when only electrons with energy above 11.55 eV are simulated with the Monte Carlo model. Indeed, the cross section rises with decreasing energy (e.g,, it is $3x10^{-17}$ cm^2 at 1000 eV and rises to 10^{-7} cm^2 at 0.01 eV), but since the density of the target particles (i.e., electrons) is 4-5 orders of magnitude lower than the Ar gas atom density, the process is, in practice, only important at electron energies of a few eV and lower [6].

To determine which collision takes place, the partial collision probabilities of the various collisions are calculated, and the total collision probability (which is equal to one, since it is the sum over all partial collision probabilities) is subdivided in intervals with lengths corresponding to these partial collision probabilities. A second random number between 0 and 1 is generated, and the interval in which the random number falls, determines the collision that takes place. Then, the new energy and direction after collision are also defined by random numbers, based on energy and angular differential cross sections [9-11] (see also refs [12-15] for more details).

This procedure is repeated for all electrons during that time-step. Then, the Monte Carlo procedure is repeated during the next time-step, again for all electrons, and so on, until (periodic) steady state is reached. However, the electrons can also be removed from the Monte Carlo model, when they undergo recombination at the cell walls, or when they are transferred to the slow electron group, which happens when their energy drops below 11.55 eV (see above). Indeed, these "slow" electrons cannot give rise to the most frequent inelastic collisions anymore, i.e., excitation and ionization from the Ar ground state; their most important role is carrying the electrical current and providing negative space charge, which can as well be described with a fluid model (see below), to save calculation time. However, when we want to calculate the detailed excitation and de-excitation between the various excited Ar and Cu levels (for the collisional-radiative models; see below), all electrons, also the slow ones, are simulated with the Monte Carlo model, because low energy electrons can cause de-excitation or excitation to nearby levels. More information about this model, developed for the dc, rf and pulsed mode, can be found in refs. [4,12-16].

Fluid Model for the Slow Electrons and Ar ions

The slow electrons are described, together with the Ar ions, in a fluid model. It is based on thermal equilibrium with the local electric field, which means that the energy gained from the electric field is locally balanced by the energy lost due to collisions. The fluid model consists of the continuity equations for ions and electrons, the transport equations for ions and electrons, an electron energy balance equation for the electrons (only used in the model when it is applied to the rf discharge, see [15,16]), and Poisson's equation to obtain the electric field distribution. Not only Ar^+ ions, but also Ar^{2+} and Ar_2^+ ions are considered in the model. This leads to 10 coupled differential equations:

$$
\begin{aligned}
&\frac{\partial n_{Ar^+}(z,r,t)}{\partial t}+\overline{\nabla}\cdot\overline{j_{Ar^+}}(z,r,t)=R_{prod,Ar^+}(z,r,t)-R_{loss,Ar^+}(z,r,t)\\
&\frac{\partial n_{Ar^{2+}}(z,r,t)}{\partial t}+\overline{\nabla}\cdot\overline{j_{Ar^{2+}}}(z,r,t)=R_{prod,Ar^{2+}}(z,r,t)-R_{loss,Ar^{2+}}(z,r,t)\\
&\frac{\partial n_{Ar_2^+}(z,r,t)}{\partial t}+\overline{\nabla}\cdot\overline{j_{Ar_2^+}}(z,r,t)=R_{prod,Ar_2^+}(z,r,t)-R_{loss,Ar_2^+}(z,r,t)\\
&\frac{\partial n_{e,slow}(z,r,t)}{\partial t}+\overline{\nabla}\cdot\overline{j_{e,slow}}(z,r,t)=R_{prod,e,slow}(z,r,t)-R_{loss,e,slow}(z,r,t)\\
&\overline{j_{Ar^+}}(z,r,t)=\mu_{Ar^+}n_{Ar^+}(z,r,t)\overline{E}(z,r,t)-D_{Ar^+}\overline{\nabla}n_{Ar^+}(z,r,t)\\
&\overline{j_{Ar^{2+}}}(z,r,t)=\mu_{Ar^{2+}}n_{Ar^{2+}}(z,r,t)\overline{E}(z,r,t)-D_{Ar^{2+}}\overline{\nabla}n_{Ar^{2+}}(z,r,t)\\
&\overline{j_{Ar_2^+}}(z,r,t)=\mu_{Ar_2^+}n_{Ar_2^+}(z,r,t)\overline{E}(z,r,t)-D_{Ar_2^+}\overline{\nabla}n_{Ar_2^+}(z,r,t)\\
&\overline{j_{e,slow}}(z,r,t)=-\mu_{e,slow}n_{e,slow}(z,r,t)\overline{E}(z,r,t)-D_{e,slow}\overline{\nabla}n_{e,slow}(z,r,t)\\
&\frac{\partial w_{e,slow}(z,r,t)}{\partial t}+\overline{\nabla}\cdot\left(\frac{5}{3}\varepsilon_{e,slow}(z,r,t)\overline{j_{e,slow}}(z,r,t)+\overline{q}(z,r,t)\right)=\\
&\qquad -e\overline{j_{e,slow}}(z,r,t)\cdot\overline{E}(z,r,t)-R_{w,e,slow}(z,r,t)\\
&\nabla^2V(z,r,t)+\frac{e}{\varepsilon_0}\left(n_{Ar^+}(z,r,t)+n_{Ar^{2+}}(z,r,t)+n_{Ar_2^+}(z,r,t)-n_{e,slow}(z,r,t)\right)=0
\end{aligned}
\qquad (3)
$$

n and j are the densities and fluxes, respectively, of the Ar ionic species and electrons. R_{prod} and R_{loss} are the production and loss rates. Production of Ar^+ ions is due to electron impact ionization, which is calculated in the electron Monte Carlo model above, as well as Ar^{2+}-electron recombination. Loss of Ar^+ ions is due to Ar^+-electron recombination, atomic to molecular ion conversion from Ar^+ to Ar_2^+, and electron impact ionization from Ar^+ to Ar^{2+}. The production processes for the Ar^{2+} ions include electron impact ionization from Ar^0 and from Ar^+ (calculated in the Monte Carlo model above). The loss processes are Ar^{2+}-electron recombination and two-electron asymmetric charge transfer with Cu^0 (which is a resonant process [17]). Production of Ar_2^+ ions is caused by Hornbeck-Molnar associative ionization of Ar atoms, as well as by atomic ion to molecular ion conversion (see above). Loss of Ar_2^+ ions is assumed to occur entirely due to dissociative recombination. Finally, production of the slow electrons is due to electron transfer to the slow electron group (calculated in the above electron Monte Carlo model), whereas loss of these electrons is due to various electron-Ar ion recombination mechanisms. The data needed to calculate the above production and loss rates can be found in ref. [18]. Further, $\overline{E}$ is the electric field and V is the electric potential. D and μ are the diffusion coefficients and mobilities, respectively, of the Ar ionic species and electrons, for which the values are given in ref. [13]. Finally, in the electron energy balance equation: $w_{e,slow}$ is the slow electron energy density ($=n_{e,slow}\varepsilon_{e,slow}$, where $\varepsilon_{e,slow}$ is the mean electron energy), q is the heat flux [15], the first term in the right-hand side describes the energy gain by the electric

field (i.e., Ohmic heating) and the second term, $R_{w,e,slow}$, represents the electron energy loss due to collisions. It should be mentioned that this electron energy balance equation is not included in our fluid model for the dc or pulsed discharge. Indeed, once the electrons are transferred to the slow electron group, which are described in the fluid model, their exact energy is not so important, because they cannot give rise to inelastic collisions (e.g., ionization) anymore. However, in the rf discharge, the slow electrons can become heated again by the oscillating rf electric field, and they can produce again ionization. Therefore, in the rf discharge, it is necessary to calculate their energy with this energy balance equation in the fluid model, to compute the ionization rate due to these electrons.

The four transport equations can be inserted into the four continuity equations, leading to a set of five (or six) coupled differential equations (i.e., including Poisson's equation, and, in the rf case, the electron energy balance equation). Due to the severe non-linearity and strong coupling of the equations, solving this model is a difficult numerical problem. The method we used was developed by Goedheer and coworkers [19], and is based on the Scharfetter-Gummel exponential scheme for the transport equations [20,21]. The basic idea is that the particle fluxes are assumed constant between mesh points, instead of the densities. The advantage of this scheme is its ability to switch between situations where either the migration component or the diffusion component of the particle flux is dominant (i.e. high and low electric field, cathode dark space (CDS) and negative glow (NG), respectively). More details about this model can be found in refs. [13-16,18].

Monte Carlo Model for the Fast Ar Ions and Atoms in the CDS

The Ar ions are not really in equilibrium with the strong electric field in the CDS (this is the region adjacent to the cathode, characterized by a strong electric field), and the fluid model is, therefore, only an approximation for the Ar ions in this region. Therefore, the Ar ions are also simulated with a Monte Carlo method in this region, which enables us to calculate the Ar ion energy distribution at the cathode, needed to calculate the amount of sputtering (see below). Only the Ar^+ ions are treated with this Monte Carlo model, because the Ar^{2+} and Ar_2^+ ions have a lower density and flux, and they play only a minor role in the sputtering process [18]. However, beside the Ar^+ ions, also the fast (i.e., non-thermal) Ar atoms (Ar^0_f), which are created from collisions of the Ar ions, are followed with this Monte Carlo model, since it was found that they play a dominant role in the sputtering process [12].

The Ar ion and fast Ar atom Monte Carlo model is similar to the electron Monte Carlo model. During successive time-steps, the trajectory of the ions and atoms is calculated by Newton's laws, and the occurrence of a collision, the nature of the collision and the new energy and direction after collision are determined by random numbers. The collision processes taken into account are elastic scattering collisions with Ar ground state atoms, for both ions and atoms, symmetric charge transfer for Ar ions (which is actually also a form of elastic collisions, because there is no change in kinetic energy [22]), and ion and atom impact ionization, excitation and de-excitation for all Ar atom levels. The cross sections for elastic collisions (with isotropic scattering and with backscattering, i.e., so-called charge transfer [22]) are adopted

from [22]. The cross sections for ionization and excitation from the Ar ground state are taken from [23]. These processes are generally not taken into account in plasma models, but they were found to be important at the high discharge voltages of 1000 V encountered in analytical glow discharges, since the cross sections increase with rising energy, reaching a maximum around 1000-10000 eV. Indeed, we found that these processes had to be incorporated in our models, in order to predict the correct current-voltage-pressure characteristics in dc analytical glow discharges [24]. Finally, the cross sections for ionization, excitation and de-excitation from excited Ar levels are described in [6]. Due to lack of data, we had to use empirical formulas to calculate these cross sections, but again, this determined only the excited level populations (to a small extent) and had no effect on the overall fast Ar ion and atom behavior. More information about this Monte Carlo model can be found in refs. [12,24,25].

Heat Transfer Model for the Ar Gas Atoms

In most cases, we have assumed that the Ar gas atoms are at rest, uniformly distributed throughout the discharge, and no specific model is applied to describe their behavior. However, recently we have developed a model for the dc glow discharge to calculate gas heating, and consequently the gas temperature distribution, which yields, when the gas pressure is constant, a non-uniform gas density distribution. The gas temperature is calculated with the heat conduction equation:

$$\frac{\partial^2 T_g}{\partial z^2} + \frac{1}{r}\frac{\partial}{\partial r}\left(r \frac{\partial T_g}{\partial r} \right) = - \frac{P}{\kappa} \qquad (4)$$

where T_g is the Ar gas temperature (function of z and r position), P is the power input and κ is the thermal conductivity (= 1.8×10^{-4} W cm^{-1} K^{-1} for Ar). The power input in the Ar gas is calculated in the ion and atom Monte Carlo models, based on collisions and subsequent energy transfer of the Ar ions, fast Ar atoms and Cu atoms (see below) to the Ar gas atoms. A detailed explanation of this model, as well as the required input data (such as the cathode temperature and thermal accommodation coefficients at the cell walls), can be found in ref. [26].

Collisional-radiative Model for the Ar Excited Atoms

A collisional-radiative model is actually a kind of fluid model, specifically applied to atoms and ions in excited levels. It consists of a set of coupled balance equations (one for each level) with various production and loss terms. Since the production and loss processes are either due to collisions or radiative decay (see below), this model is called "collisional-radiative model".

Figure 1 shows a schematic energy diagram of the Ar atomic levels taken into account in this model. 64 Ar atomic excited levels are considered; most of them are effective levels, i.e., a group of individual levels with comparable excitation energy and quantum numbers. The four 4s levels (i.e., two metastable levels and two resonant levels) are, however, treated separately.

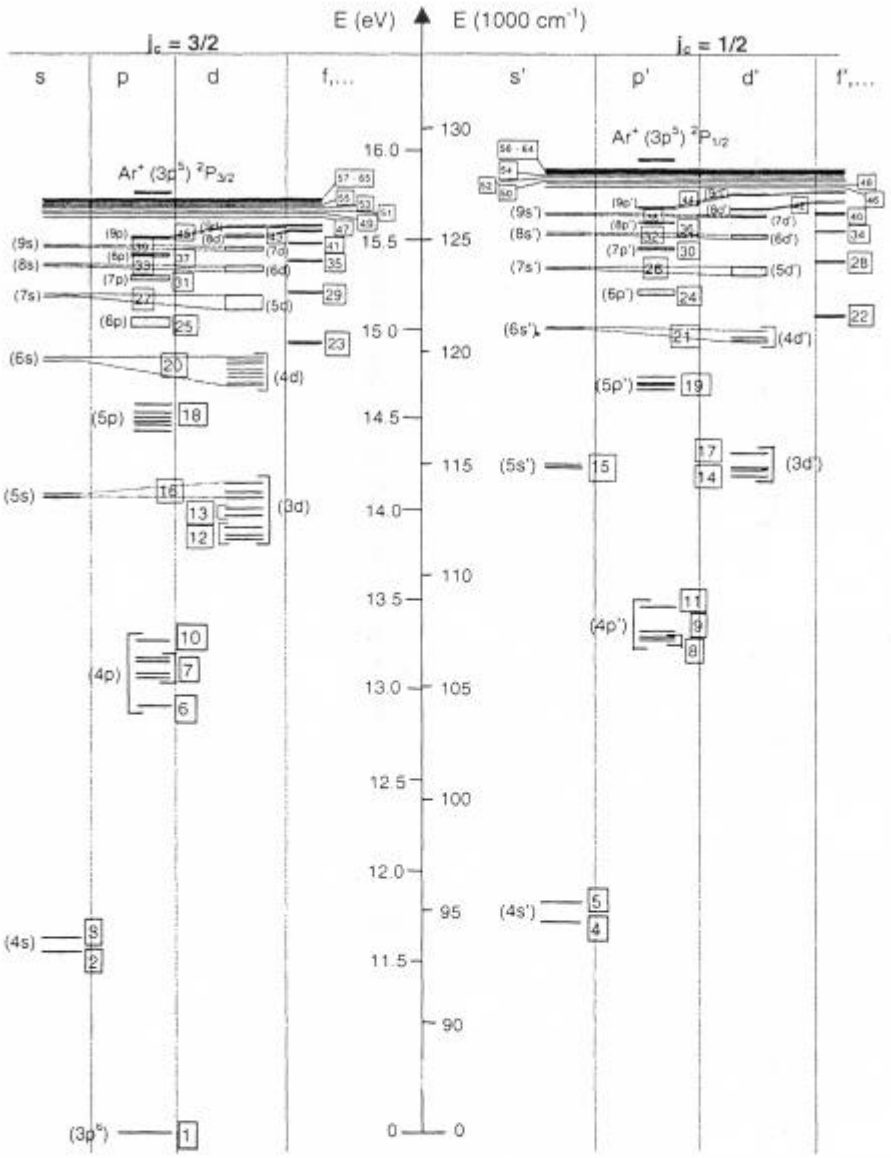

FIGURE 1. Energy level scheme of the Ar atoms, illustrating all the effective levels incorporated in the collisional-radiative model [6].

The behavior of the levels is described with 64 coupled balance equations, taking into account a large number of populating and depopulating processes:

$$\frac{\partial n_{Ar^*}(z,r,t)}{\partial t} - D_{Ar^*}\frac{1}{r}\frac{\partial}{\partial r}\left(r\frac{\partial n_{Ar^*}(z,r,t)}{\partial r}\right) - D_{Ar^*}\frac{\partial^2 n_{Ar^*}(z,r,t)}{\partial z^2} = R_{prod}(z,r,t) - R_{loss}(z,r,t) \tag{5}$$

The production and loss processes taken into account are: electron, Ar ion and atom impact ionization from all levels, excitation and de-excitation between all the levels,

and electron-ion three-body and radiative recombination to all levels, as well as radiative decay between the levels and Hornbeck-Molnar associative ionization (for Ar* levels with excitation energy above 14.7 eV). Moreover, some additional processes are incorporated for the 4s metastable levels, i.e., metastable atom - metastable atom collisions, Penning ionization of the sputtered Cu atoms, and two-body and three-body collisions with Ar ground state atoms. The cross sections and rate coefficients of all these processes are discussed in detail in ref. [6]. As mentioned before, the cross sections for electron, ion and atom impact ionization and excitation are mainly determined from empirical formulas. The cross sections for electron impact de-excitation and for electron-ion recombination are obtained from the corresponding electron impact excitation and ionization cross sections, based on the principle of detailed balancing. The Einstein transition probabilities for the 4s-4p and 4s-5p transitions (which dominate the spectrum [27]) were obtained from [28], whereas the values for other (less important) transitions were calculated on the basis of intermediate and (j,K) coupling [29]. Hornbeck-Molnar associative ionization was initially not incorporated in the model [6], but was added later on (when the behavior of Ar_2^+ ions was described; see details in [18]), and it was found to be important for the levels above 14.71 eV [30]. Finally, the additional data for the processes concerning the 4s metastable levels, i.e., metastable atom – metastable atom collisions, two-body and three-body collisions with Ar atoms, and Penning ionization, are taken from the literature [31-34]. It should be mentioned that the rate coefficient for Penning ionization between Ar metastable atoms and sputtered Cu atoms was difficult to find in the literature. We used an empirical formula [33], which was fitted to some experimentally obtained cross sections for certain elements (e.g., Zn, Cd and Mg) [33,34] in order to arrive at approximate values for other elements, like Cu. It is clear that most of these input data in the model are subject to large uncertainties, which will be reflected in the excited level populations. However, the optical emission intensities which we calculated from the excited level populations appeared to be in reasonable agreement with experimental data (see [27]) which suggests that the above data are not so critical for a realistic description of the excited Ar atoms.

Transport of the atomic levels occurs, in principle, by diffusion. However, the latter plays only a role for the 4s levels, because the higher excited levels decay more rapidly to the ground state by emission of radiation, than they could move due to diffusion. Furthermore, when the two non-metastable 4s levels decay to the ground state, a large fraction of the emitted radiation is again re-absorbed by the ground level, leading again to formation of this 4s level. This phenomenon of "radiation trapping" is accounted for by means of "escape factors" which express the fraction of photons that can really escape without being re-absorbed [35,36]. The escape factors we used were calculated, based on combined Doppler and collisional line broadening [6].

The 64 balance equations are coupled to each other, because higher and lower levels affect each other due to radiative decay, excitation and de-excitation. The boundary conditions for these equations are $n_{Ar^*}=0$ at all walls, because the excited levels will de-excite upon collision at the walls. More information about this model can be found in refs [6,30] for the dc and the rf case, respectively.

Cathode Sputtering and Thermalization of the Sputtered Atoms

The flux of sputtered Cu atoms, J_{sput}, is calculated from the energy distribution functions of the Ar ions, fast Ar atoms and Cu ions (see below) bombarding the cathode ($f_0(E)$; calculated in the Monte Carlo models), multiplied with an empirical formula for the sputtering yield as a function of the bombarding energy (Y(E) [37]):

$$J_{sput} = -\int_E \left\{ Y_{Ar-Cu}(E) \left[f_{0,Ar^+}(E) + f_{0,Ar_f^0}(E) \right] + Y_{Cu-Cu}(E) f_{0,Cu^+}(E) \right\} dE \qquad (6)$$

When the Cu atoms are sputtered from the cathode, they have energies in the order of 5-10 eV. However, they lose these energies almost immediately in the first mm's from the cathode, by collisions with Ar gas atoms, until they are thermalized. This thermalization process is described with a Monte Carlo model, similar to the electron Monte Carlo model (see above), except that the electric field does not come into play for the neutral atoms, and that only elastic collisions with Ar atoms are incorporated. Indeed, collisions with other plasma species could be neglected, due to the lower densities of these species. This Monte Carlo model is run until all atoms are thermalized, and it results in a so-called thermalization profile, F_T, i.e., the number of atoms thermalized as a function of position from the cathode. More details about the collision cross sections and the scattering formulas can be found in ref. [38].

The product of J_{sput} and F_T will be used as source term for the Cu atoms, described in the following model.

Collisional-radiative Model for the Cu Atoms and Ions

The further behavior of the thermalized Cu atoms (i.e., transport, ionization and excitation), and the behavior of the excited Cu atoms and of the Cu ions (in the ground state and in excited levels) is described with a collisional-radiative model. Eight Cu atom levels, seven Cu^+ ion levels and the Cu^{++} ions are considered (see the energy level scheme in figure 2). Some of the Cu atom and ion levels are grouped into effective levels. The behavior of all the levels is again described with a set of coupled balance equations with various production and loss terms, i.e., electron and atom impact ionization from all levels, excitation and deexcitation between all levels, radiative decay between all levels, electron-ion three-body recombination to the upper Cu atom and Cu ion levels, Penning ionization by Ar metastable atoms, and asymmetric charge transfer between Cu atoms and Ar ions. Moreover, an additional production term for the Cu ground state atoms is the product of J_{sput} and F_T, as is described above.

The transport occurs by diffusion for the atoms, and by diffusion and migration for the ions. The equations are also coupled due to the effect of higher and lower levels on each other. More information about this model can be found in refs. [7,39], as well as about the input data needed to calculate all the production and loss processes (which are mainly taken from the literature concerning Cu vapor lasers; see e.g., [40,41]).

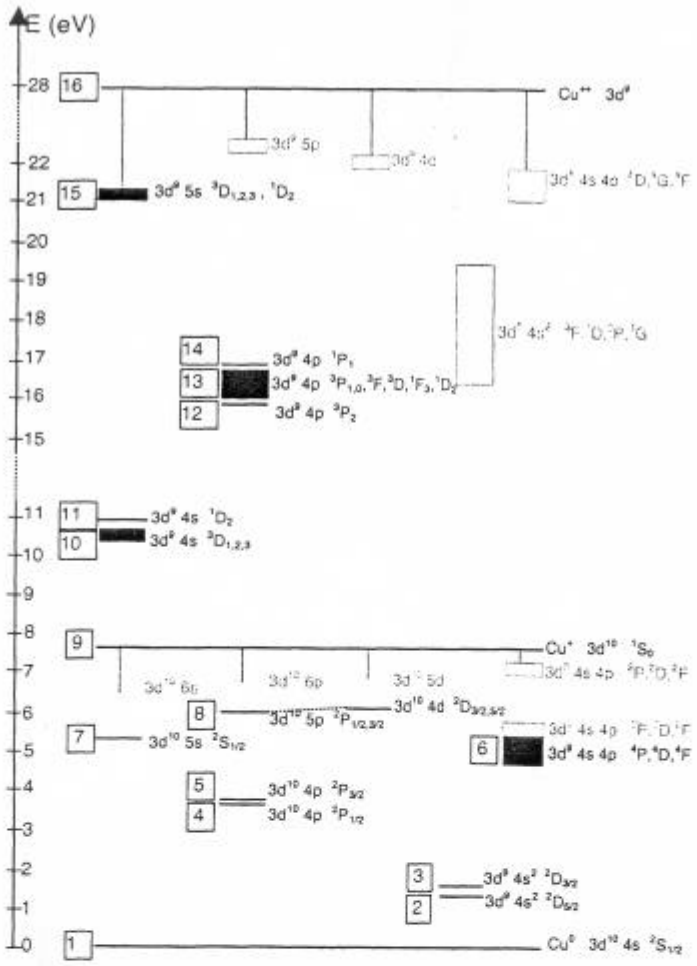

FIGURE 2. Energy level scheme of the Cu atoms and ions [7]. The levels considered in the model are presented in black. Reprinted from [7] with permission of Elsevier Science.

Monte Carlo Model for the Cu Ions in the CDS

Finally, the Cu ions are also treated with a Monte Carlo model in the CDS, because they are not in equilibrium with the strong electric field in this region. The procedure is again comparable to the electron Monte Carlo model (i.e., calculation of the trajectory by Newton's laws, and treatment of the collisions by random numbers); see refs. [42,43] for more information.

Coupling of the Models

All the models are coupled to each other due to the interactions between the various plasma species, i.e., the output of one model is used as input for the other models. The models are solved iteratively until final convergence is reached, to obtain an overall picture of the glow discharge. A schematic picture of the coupling procedure is given in ref. [44,45]. The whole calculation procedure takes several days on a unix professional workstation.

TYPICAL RESULTS OF THE MODELS

Table 2 presents an overview of typical results obtained with the models. All these plasma quantities can be calculated for different discharge conditions (voltage, current, power, pressure), operation modes (dc, rf or pulsed) and cell geometries (see e.g., [46-48]). To test the validity of the models, the calculated quantities must be compared with experimental data. Such a comparison has been carried out for some quantities (when experimental data were available; see Table 2), and in general, reasonable agreement between experimental and calculated results was reached.

Some of the characteristic calculated plasma quantities are illustrated in Figure 3, for a simplified analytical glow discharge cell geometry of 1 cm length, at typical discharge conditions used for GDMS (i.e., dc discharge at 1000 V, 3 mA, 0.5 Torr). The discharge consists of three regions (see part a): a cathode dark space (CDS, adjacent to the cathode), a negative glow (NG, which fills the main part of the discharge), and an anode dark space (ADC, adjacent to the anode).

The calculated potential and electric field distributions are shown in part (b). The potential (solid line, left axis) is -1000 V at the cathode and increases to zero at about 0.24 cm from the cathode. The position where the potential crosses the zero-line is defined as the interface between CDS and NG. The potential is slightly positive in the NG (i.e., a few V; which is called the plasma potential) and decreases to zero at the anode. Hence, the NG is the most positive part of the discharge. The electric field (dashed line, right axis) is extremely negative at the cathode (-8 kV/cm) and increases almost linearly in the CDS. It does not cross the zero-line at the CDS-NG interface but bends off to a small negative value in the NG. It goes through zero at about 0.7 cm and then takes small positive values. Close to the anode it rises to about 200 V/cm.

Parts (c) and (d) present the density profiles of the various plasma species. The Ar metastable atom density (part (c), dashed line, left axis) reaches a maximum of about 10^{12} cm^{-3} rather close to the cathode and decreases to low values in the rest of the discharge. The Ar ion density (part (c), solid line, left axis) is low and more or less constant in the CDS and reaches a broad maximum of about $5x10^{11}$ cm^{-3} halfway the discharge, whereafter it decreases to a low value at the anode. The slow electron density (part (c), solid line, left axis) is zero in the CDS and close to the anode and it is almost equal to the Ar ion density in the NG. This gives rise to a net positive space charge in the CDS and close to the anode and nearly charge neutrality in the NG. The latter defines the characteristic potential and electric field distributions presented in part (b). The fast electron density (part (c), solid line, right axis) reaches a maximum in the beginning of the NG; it is, however, four orders of magnitude lower than the Ar ion and slow electron densities, and hence does not contribute to the space charge. The sputtered Cu atom density (part (d), left axis) is at its maximum (ca. $6x10^{12}$ cm^{-3}) close to the cathode and decreases almost linearly towards the anode. The Cu ion density (part (d), right axis) shows the same profile shape as the Ar ion density but is about two orders of magnitude lower. From part (d) it can also be deduced that the ionization degree of sputtered Cu atoms (i.e., the ratio of Cu ion to Cu atom density) is of the order of 0.1 %. This calculated value should not be considered too strictly; it depends strongly on the discharge conditions, cell geometry and kind of cathode material; for other conditions, values in the order of a few % were calculated [46,55].

TABLE 2. Overview of the Typical Results Obtained with our Models, and Comparison with Experimental Data, if Available.

Calculated Quantities (+ references for more information)		References for Comparison with Experiment
Electrical characteristics:		
Current as function of voltage and pressure (dc)	24,44,46	24,44
Rf amplitude and dc bias voltage (rf)	16	49
Voltage, current, power as function of time (pulsed)	4	50
Potential, electric field distributions:		
3D potential distributions	4,13-16,44	-
3D axial and radial electric field distributions	4,13-16,44	-
Lengths of the different regions (CDS, NG)	4,13-16,44	51 (Aston formula)
3D density profiles of:		
* Ar atoms (gas heating)	26	-
* Ar^+, Ar^{2+} and Ar_2^+ ions	4,13-16,18,44	-
* fast Ar atoms	12,44	-
* Ar metastable atoms	6,30,43,44,52	53 (LIF)
* other Ar excited levels	6,30	-
* fast electrons	12-14,44	-
* thermal electrons	4,13-16,44	54 (Langmuir probe)
* atoms of the cathode material	7,39,42-44	55 (LIF)
* ions of the cathode material	7,39,42-44	55 (LIF)
* cathode atoms + ions in excited levels	7,39	
Ion fluxes of various Ar and cathode ions at the exit slit of the cell to the mass spectrometer	18,47,48	47,56 (ratios in glow discharge mass spectra)
Ionization degrees of Ar and cathode atoms	42-44	55 (based on LIF results)
3D energy distributions and mean energies of:		
* electrons	12,13,15,44	-
* Ar ions	12,25,44	57 (at cathode)
* fast Ar atoms	12,25,44	-
* cathode ions	42,44	57 (at cathode)
Information about collision processes:		
* collision rates of the various collision processes of electrons, Ar^+ ions and fast Ar atoms	4,12-16,24,44	-
* rates of Penning ionization, asymmetric charge transfer and electron impact ionization of sputtered atoms; relative contributions to the total ionization	7,39,42-44	-
* rates and relative contributions of the various populating and depopulating processes (see text) of the metastable and other excited Ar levels	6,30,43,44,52	-
* rates and relative contributions of the various populating and depopulating processes (see text) of the excited Cu atom + ion levels	7,39	-
Information about sputtering:		
* Sputtering (erosion) rates at the cathode	39,44,46,58	59,60
* Thermalization profiles of the sputtered atoms	38,44	-
* Amount of redeposition on the cathode by backscattering or backdiffusion	38,44,58	-
* Relative contributions of Ar ions, fast Ar atoms and cathode ions to the sputtering process	12,39,42-44	-
* 2D crater profiles due to sputtering at the cathode	58	59
Emission spectra and spatial distributions of emission intensities for Ar and Cu atoms + ions	27,61,62	27,62
Effect of cell geometry	47,48	-

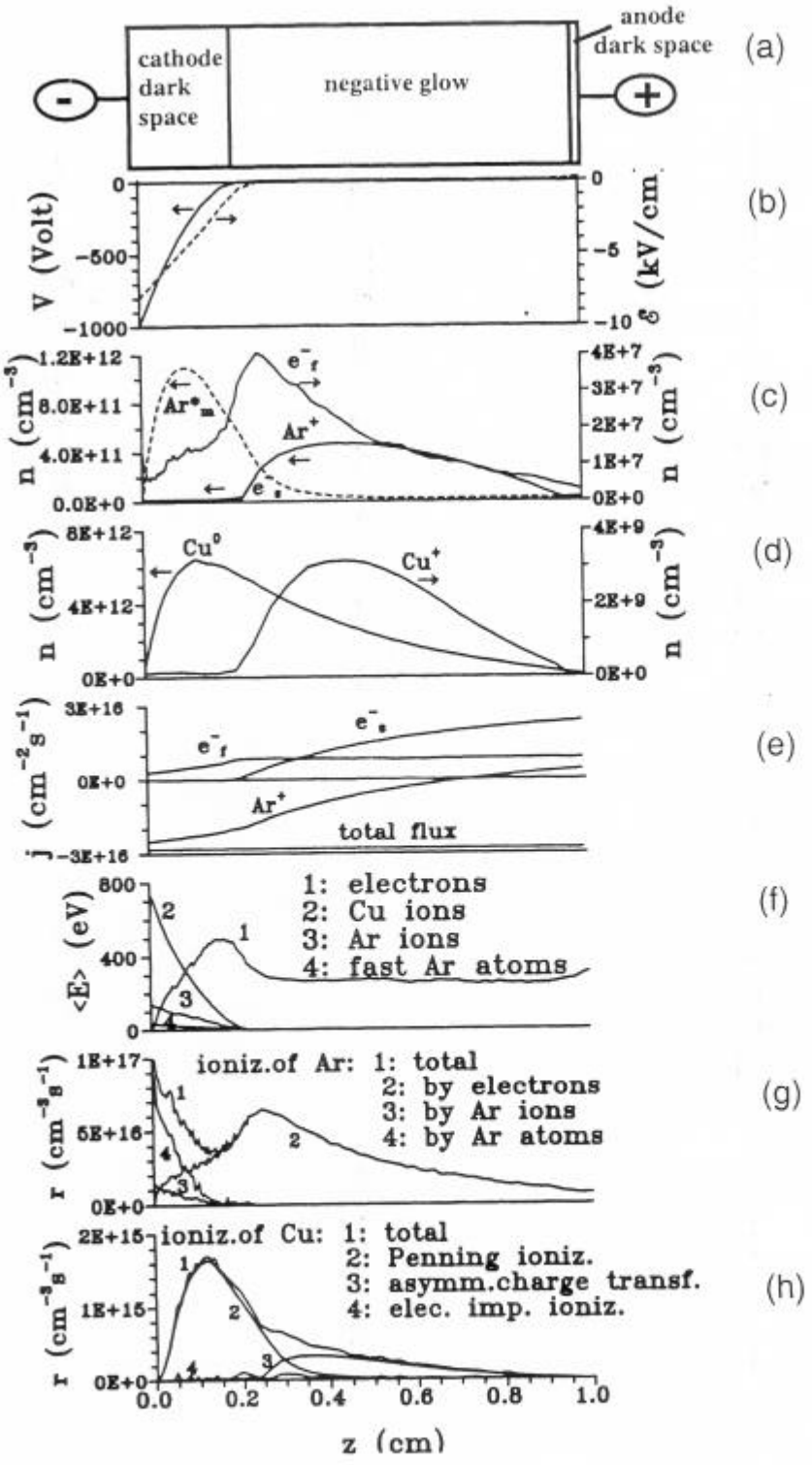

FIGURE 3. Calculated characteristic plasma quantities in one dimension, at 1000 V, 3 mA and 0.5 Torr (dc conditions). (a) discharge geometry; (b) potential and electric field distributions; (c) number density profiles of Ar metastable atoms (Ar_m^*), Ar^+ ions and slow (e^-_s) and fast (e^-_f) electrons; (d) number density profiles of sputtered Cu^0 atoms and Cu^+ ions; (e) fluxes of Ar^+ ions, fast and slow electrons, and total flux flowing through the discharge; (f) mean energies of electrons, Cu ions, Ar ions and fast Ar atoms throughout the discharge; (g) ionization rates of Ar atoms (total + individual processes); (h) ionization rates of Cu atoms (total + individual processes).

The fluxes of the dominant current carriers are indicated in part (e). In the CDS most of the current is carried by the Ar ions, which are directed towards the cathode by the strong electric field in front of it. The fast electron flux at the cathode is about an order of magnitude lower than the Ar ion flux (determined by the ion induced secondary electron emission coefficient, which is in the order of 0.1) and it is in the opposite direction (i.e., away from the cathode). It increases in the CDS and remains nearly constant in the NG. The slow electron flux, on the other hand, is zero in the CDS. Indeed, slow electrons are assumed not to be present in this region since they would immediately be accelerated by the electric field and they would not remain in the slow group. Their flux increases, however, considerably in the NG, as more and more fast electrons are slowed down by collisions and are transferred to the slow electron group. In the NG, most of the current is carried by the (slow) electrons. The Ar ion flux changes sign in this region; hence Ar ions will bombard the anode as well.

Part (f) shows the mean energies of electrons, Cu ions, Ar ions and fast Ar atoms, as a function of distance from the cathode. The electrons (no. 1) start at the cathode with rather low energies, and they gain energy in the CDS from the electric field. They lose, however, also energy by collisions, so that their mean energy at the CDS-NG interface is not equal to the discharge voltage, but is about 50 % of this value. The electron energy decreases in the NG, since the electrons do not gain energy from the electric field anymore (which is very small, see part (b)) but they lose their energy more efficiently due to collisions. Further in the NG, the electron energy remains more or less constant since the electrons travel back and forth in this region. The Cu ions, Ar ions and fast Ar atoms are more or less thermalized in the NG, but their energy increases as they move towards the cathode. The mean Cu ion energy (no. 2) at the cathode is about 700 eV (hence about 70 % of the discharge voltage), since the Cu ions do not lose their energy very efficiently by collisions. Indeed, they are only subject to elastic collisions with Ar atoms; asymmetric charge transfer collisions with Ar atoms have a lower cross section, and symmetric charge transfer with Cu atoms is of low probability due to the much lower Cu atom density compared to Ar atom density (the latter is ca. 10^{16} cm^{-3}). The Ar ions (no. 3), on the other hand, reach a maximum mean energy of only about 150 eV (i.e., 15 % of the discharge voltage) at the cathode, since these species lose the energy they gained from the electric field very efficiently due to symmetric charge transfer collisions with Ar atoms. The mean energy of the fast Ar atoms (no. 4) at the cathode is only in the order of 30 eV (ca. 3 % of the discharge voltage). Indeed, these species are created from the Ar ions with energies corresponding to the Ar ion energies, but they cannot gain more energy from the electric field. It should be mentioned that the term "fast" Ar atoms is used for those atoms which are not thermalized, and have energies higher than ca. 0.05 eV.

From the energies and the fluxes of the species bombarding the cathode (i.e., Ar ions, fast Ar atoms and Cu ions), the amount of sputtering can be calculated. It is generally found that the flux of fast Ar atoms bombarding the cathode is definitely higher than the fluxes of Ar ions and Cu ions. Therefore, the fast Ar atoms play a dominant role in sputtering [12]. However, the efficiency of sputtering increases with the energy of the bombarding particles and with their mass [37]; therefore, it is expected that the contribution of Cu ions to sputtering (so-called self-sputtering) is non-negligible, in spite of their lower total flux, and this contribution rises

significantly with pressure and voltage. It was calculated that the fast Ar atoms, Ar ions and Cu ions contribute for about 30-70 %, 20-30 % and 0.1-50 % to the sputtering, respectively, at the typical discharge conditions used in analytical glow discharges (i.e., 600-1200 V, 1-50 mA, 1-5 Torr) [44,46].

Finally, parts (g) and (h) of Figure 3 present the ionization rates of Ar atoms and Cu atoms, respectively. The Ar atoms are mainly ionized by electron impact ionization, but fast Ar ion and atom impact ionization play also a role in the CDS, especially close to the cathode where the Ar ions and atoms reach their maximum energy (see part (f)). Integrated over the entire discharge region, electron, fast Ar ion and atom impact ionization contribute for about 90 %, 2 % and 8 %, respectively, to the ionization of Ar. A more or less similar figure can be made for the excitation rate of Ar atoms, with a maximum adjacent to the cathode due to fast Ar ion and atom impact excitation and a second peak in the beginning of the NG caused by electron impact excitation. This corresponds well with the luminous intensity throughout the glow discharge: the NG is the most luminous part of the discharge, but close to the cathode, a bright layer is often observed, called the cathode glow. For the ionization of sputtered Cu atoms, Ar ion and atom impact ionization are not included in the model, basically because no cross sections are available in the literature and also because these processes are probably not important for the general ionization of Cu atoms. Indeed, besides electron impact ionization, two other processes come into play for the sputtered atoms, i.e., Penning ionization by Ar metastable atoms and asymmetric charge transfer with Ar ions. Both these processes seem to be more important than electron impact ionization. The relative contributions of Penning ionization, asymmetric charge transfer and electron impact ionization, integrated over the entire discharge region, were calculated to be about 60 %, 36 % and 4 %, respectively, at the discharge conditions of 1000 V and 3 mA. These values are only approximate, because the rate coefficients of Penning ionization and especially of asymmetric charge transfer are subject to uncertainties. Moreover, these calculated contributions depend strongly on the discharge conditions, cell dimensions and especially kind of sputtered material. Nevertheless, we found for all conditions investigated that Penning ionization and asymmetric charge transfer were more important than electron impact ionization. Since the latter process is the dominant one for Ar atoms (see above), it follows that the sputtered atoms are more efficiently ionized than the Ar atoms. Indeed, we calculated typical ionization degrees of 10^{-5}-10^{-3} for Ar, and in the order of 10^{-4}-5×10^{-2} for the sputtered atoms (Cu, Ta, ...).

CONCLUSION

A hybrid modeling network has been developed, consisting of Monte Carlo, fluid and collisional-radiative models to describe the various species in glow discharge plasmas. The different submodels are explained, and the data needed to solve the models are discussed. It is clear that the modeling network requires a large number of input data. Some of them are rather well-known (e.g., electron impact ionization and excitation cross sections from the Ar ground state), but most of them are subject to large uncertainties (e.g., the cross sections for excitation and ionization from various

Ar and Cu excited levels). Fortunately, the latter data do not affect the overall model calculations to a large extent; they determine only the excited level populations. The data which have the largest influence on the overall model calculations are the electron, Ar ion and atom impact ionization cross sections from the Ar ground state (of which the first is well-known, but the two others are subject to larger uncertainties), as well as the gas pressure and temperature (of which the latter is also generally unknown, and can be significantly higher than room temperature [26]). Indeed, these data determine the number of ionization collisions, and hence the creation of electrons and Ar ions, and therefore also most other collision rates, and the densities, fluxes and energies of the various plasma species, as well as the total electrical current. Nevertheless, it has been shown that the calculated current is in reasonable agreement with experimental values, which suggests that the input data used in the model are sufficiently reliable.

In order to show the possibilities of the model network, an overview is given of the typical results that have been calculated, and some of them are illustrated. Reasonable agreement has been reached between the model results and experimental data, which suggests that our models present a realistic picture of the analytical glow discharge.

ACKNOWLEDGMENTS

A. Bogaerts is indebted to the Fund for Scientific Research (FWO) Flanders for financial support. The authors also acknowledge financial support from the Federal Services for Scientific, Technical and Cultural Affairs (DWTC/SSTC) of the Prime Minister's Office through IUAP-IV (Conv. P4/10). Finally, they would also like to thank W. Goedheer, J. Vlcek and R. Carman for their cooperation in developing the models.

REFERENCES

1. Marcus, R.K. (ed.), *Glow Discharge Spectroscopies*, New York: Plenum Press, 1993.
2. Bogaerts, A., and Gijbels, R., *J. Anal. At. Spectrom.* **13,** 945-953 (1998).
3. Bogaerts, A., and Gijbels, R., *J. Anal. At. Spectrom.* **15**, (in press: 2000).
4. Bogaerts, A., and Gijbels, R., *J. Anal. At. Spectrom.* (submitted).
5. Phelps, A.V., and Petrovic, Z. Lj., *Plasma Sources Sci. Technol.* **8**, R21-R44 (1999).
6. Bogaerts, A., Gijbels, R., and Vlcek, J., *J. Appl. Phys.* **84,** 121-136 (1998).
7. Bogaerts, A., Gijbels, R., and Carman, R. J., *Spectrochim. Acta B* **53,** 1679-1703 (1998).
8. Hashiguchi, S., *IEEE Trans. Plasma Sci.* **19**, 297-300 (1991).
9. Boeuf, J.P., and Marode, E., *J. Phys. D* **15**, 2169-2187 (1982)
10. Surendra, M., Graves, D.B., and Jellum, G.M., *Phys. Rev. A* **41**, 1112-1125 (1990).
11. Hasted, J.B., *Physics of Atomic Collisions*, London: Butterworth, 1972.
12. Bogaerts, A., van Straaten, M., and Gijbels, R., *Spectrochim. Acta B* **50**, 179-196 (1995).
13. Bogaerts, A., Gijbels, R., and Goedheer, W. J., *J. Appl. Phys.* **78,** 2233-2241 (1995).
14. Bogaerts, A., Gijbels, R., and Goedheer, W. J., *Anal. Chem.* **68,** 2296-2303 (1996).
15. Bogaerts, A., Gijbels, R., and Goedheer, W. J., *Jpn. J. Apl. Phys.*, **38,** 4404-4415 (1999).
16. Bogaerts, A., Yan, M., Gijbels, R., and Goedheer, W. *J., Appl. Phys.*, **86**, 2990-3001 (1999).
17. Jogwich, M., Huber, B.A., and Wiesemann, K., *Z. Phys.D*, **17,** 171-179 (1990).
18. Bogaerts, A., and Gijbels, R., *J. Appl. Phys.*, **86**, 4124-4133 (1999).
19. Passchier, J.D.P., and Goedheer, W.J., *J. Appl. Phys.* **73**, 1073-1079 (1993).

20. Gummel, H. K., *IEEE Trans. Plasma Sci,* **11**, 455-465 (1964).
21. Scharfetter, D. L., and Gummel, H. K. *IEEE Trans. Electron. Devices* **16,** 64-77 (1969).
22. Phelps, A.V., *J. Appl. Phys.* **76**, 747-753 (1994).
23. Phelps, A.V., *J. Phys. Chem. Ref. Data* **20**, 557-573 (1991).
24. Bogaerts, A., and Gijbels, R., *J. Appl. Phys.* **78,** 6427-6431 (1995).
25. Bogaerts, A., and Gijbels, R., *IEEE Trans. Plasma Sci.* **27**, 1406-1415 (1999).
26. Bogaerts, A., Gijbels, R., and Serikov, V.V., *J. Appl. Phys.* **87**, (in press: 15 June 2000).
27. Bogaerts, A., Gijbels, R., and Vlcek, J., *Spectrochim. Acta B* **53,** 1517-1526 (1998).
28. Wiese, W.L., Brault, J.W., Danzmann, K., Helbig, V., and Kock, M., *Phys. Rev. A* **39**, 2461-2471 (1989).
29. Vlcek, J., *J. Phys. D* **22**, 623-631 (1989).
30. Bogaerts, A., and Gijbels, R., *Spectrochim. Acta B* **55**, 263-278 (2000).
31. Ferreira, C.M., Loureiro, J., and Ricard, A., *J. Appl. Phys.* **57**, 82-90 (1984).
32. Tachibana, K., *Phys. Rev. A* **34**, 1007-1015 (1986).
33. Riseberg, L.A., Parks, W.F., and Schearer, L.D., *Phys. Rev. A* **8**, 1962-1968 (1973).
34. Inaba, S., Goto, T., and Hattori, S., *J. Phys. Soc. Jpn.* **52**, 1164-1167 (1983).
35. Holstein, T., *Phys. Rev.* **83,** 1159-1168 (1951).
36. Walsh, P. J., *Phys. Rev.* **116,** 511-515 (1959).
37. Matsunami, N., Yamamura, Y., Itikawa, Y., Itoh, N., Kazumata, Y., Miyagawa, S., Morita, K., Shimizu, R., and Tawara, H., *Atom. Data Nucl. Data Tables* **31**, 1-80 (1984).
38. Bogaerts, A., van Straaten, M., and Gijbels, R., *J. Appl. Phys.* **77,** 1868-1874 (1995).
39. Bogaerts, A., and Gijbels, R., *Spectrochim. Acta B* **55**, 279-297 (2000).
40. Carman, R.J., Brown, D.J.W., and Piper, J.A., *IEEE J. Quant. Electron.* **30**, 1876-1895 (1994).
41. Carman, R.J., *Opt. Lett.* **21**, 872-874 (1996).
42. Bogaerts, A., and Gijbels, R., *J. Appl. Phys.* **79,** 1279-1286 (1996).
43. Bogaerts, A., and Gijbels, R., *Anal. Chem.* **68,** 2676-2685 (1996).
44. Bogaerts, A., *Ph.D. Dissertation*, University of Antwerp (1996).
45. Bogaerts, A., and Gijbels, R., *Plasma Phys. Reports* **24**, 573-583 (1998).
46. Bogaerts, A., and Gijbels, R., *Spectrochim. Acta B* **53,** 437-462 (1998).
47. Bogaerts, A., and Gijbels, R., *J. Anal. At. Spectrom.* **12,** 751-759 (1997).
48. Bogaerts, A., and Gijbels, R., *J Am. Soc. Mass Spectrom.* **8,** 1021-1029 (1997).
49. Hoffmann, V., private communication.
50. Yang, C., and Harrison, W.W., private communication.
51. Aston, F. W., *Proc. Roy. Soc. London, Ser. A* **79,** 80 (1907).
52. Bogaerts, A., and Gijbels, R., *Phys. Rev. A* **52**, 3743-3751 (1995).
53. Bogaerts, A., Guenard, R.D., Smith, B.W., Winefordner, J.D., Harrison, W.W., and Gijbels, R., *Spectrochim. Acta B* **52,** 219-229 (1997).
54. Bogaerts, A., Quentmeier, A., Jakubowski, N., and Gijbels, R., *Spectrochim. Acta B* **50,** 1337-1349 (1995).
55. Bogaerts, A., Wagner, E., Smith, B.W., Winefordner, J.D., Pollmann, D., Harrison, W.W., and Gijbels, R., *Spectrochim. Acta B* **52,** 205-218 (1997).
56. Kennis, P., *Ph.D. Dissertation*, University of Antwerp (1996).
57. van Straaten, M., Bogaerts, A., and Gijbels, R., *Spectrochim. Acta B* **50,** 583-605 (1995).
58. Bogaerts, A., and Gijbels, R., *Spectrochim. Acta B* **52,** 765-778 (1997).
59. Jonkers, C., *Ph.D. Dissertation*, University of Antwerp (1995).
60. Bengtson, A., and Lundholm, M., *J. Anal. At. Spectrom.* **3,** 879-882 (1988).
61. Bogaerts, A., and Gijbels, R., *J. Anal. At. Spectrom.* **13,** 721-726 (1998).
62. Bogaerts, A., Donko, Z., Kutasi, K., Bano, G., Pinhao, N., and Pinheiro, M., *Spectrochim. Acta B*, (submitted).